Cell

Decision Making at a Subcellular Level Determines the Outcome of Bacteriophage Infection

Lanying Zeng,[1] Samuel O. Skinner,[1] Chenghang Zong,[1] Jean Sippy,[4] Michael Feiss,[4] and Ido Golding[1,2,3,*]
[1]Department of Physics
[2]Center for the Physics of Living Cells
University of Illinois, Urbana, IL 61801, USA
[3]Verna and Marrs McLean Department of Biochemistry and Molecular Biology, Baylor College of Medicine, Houston, TX 77030, USA
[4]Department of Microbiology, Roy J. and Lucille A. Carver College of Medicine, University of Iowa, Iowa City, IA 52242, USA
*Correspondence: igolding@illinois.edu
DOI 10.1016/j.cell.2010.03.034

SUMMARY

When the process of cell-fate determination is examined at single-cell resolution, it is often observed that individual cells undergo different fates even when subject to identical conditions. This "noisy" phenotype is usually attributed to the inherent stochasticity of chemical reactions in the cell. Here we demonstrate how the observed single-cell heterogeneity can be explained by a cascade of decisions occurring at the subcellular level. We follow the postinfection decision in bacteriophage lambda at single-virus resolution, and show that a choice between lysis and lysogeny is first made at the level of the individual virus. The decisions by all viruses infecting a single cell are then integrated in a precise (noise-free) way, such that only a unanimous vote by all viruses leads to the establishment of lysogeny. By detecting and integrating over the subcellular "hidden variables," we are able to predict the level of noise measured at the single-cell level.

INTRODUCTION

Living cells integrate signals from their environment to make fate-determining decisions (Alon, 2007). When examined at the single-cell level, the process of cellular decision making often appears imprecise or "noisy," in the sense that individual cells in a clonal population undergo different fates even when subject to identical conditions (Arkin et al., 1998; Blake et al., 2003, 2006; Chang et al., 2008; Elowitz and Leibler, 2000; Kærn et al., 2005; Losick and Desplan, 2008; Maamar et al., 2007; Singh and Weinberger, 2009; Spencer et al., 2009; Suel et al., 2007; Yamanaka, 2009). In the literature, this cell-fate heterogeneity has largely been attributed to the inherent stochasticity of chemical reactions in the cell, especially the reactions governing gene expression (Losick and Desplan, 2008; Raj and van Oudenaarden, 2008; Singh and Weinberger, 2009). In recent years, considerable progress has been made toward understanding the sources and characteristics of this stochasticity. For example, the fact that both transcription (Chubb et al., 2006; Golding et al., 2005; Raj et al., 2006) and translation (Cai et al., 2006; Yu et al., 2006) occur in a bursty, non-Poissonian manner implies that cell-to-cell variations in protein levels are higher than previously assumed. In another line of investigation, the role of stochastic gene expression in cell-fate decisions has been directly demonstrated and quantified (Cagatay et al., 2009; Maamar et al., 2007; Suel et al., 2007).

At the same time, however, a competing view regarding the source of cell-fate heterogeneity is that what seems like an imprecise decision by the cell may largely reflect our own inability to measure some "hidden variables," i.e., undetected differences between individual cells, which deterministically set the outcome of cellular decision making. As two recent works have shown (Snijder et al., 2009; St-Pierre and Endy, 2008), careful quantification of cell-to-cell differences can in some cases "explain away" some—but not all—of the observed cell-fate heterogeneity without the need to invoke chemical stochasticity. So far, the two lines of evidence regarding cell-fate heterogeneity have existed in parallel, and have not been reconciled within a single quantitative narrative of how stochasticity and "hidden variables" combine to produce the observed single-cell phenotype.

Here we use the decision between dormancy (lysogeny) and cell death (lysis) following infection of *E. coli* by bacteriophage lambda to demonstrate how a cascade of decisions at the subcellular level gives rise to the "noisy" phenotype observed at the single-cell level. We follow viral infection at the level of individual phages and cells. We find that, upon infection of the cell by multiple phages, a choice between lysis and lysogeny is first made at the level of each individual phage dependent on the total viral concentration inside the cell. The decisions by all viruses infecting a single cell are then integrated in a precise (noise-free) way, such that only a unanimous "vote" by all viruses leads to the establishment of lysogeny. By integrating over the subcellular degrees of freedom (number and location of infecting phages, cell volume), we are able to reproduce the observed whole-cell phenotype and predict the observed level of noise in the lysis/lysogeny decision.

Upon infection of an *E. coli* cell by bacteriophage lambda, a decision is made between cell death (lysis) and viral dormancy (lysogeny) (Ptashne, 2004), a process that serves as a simple paradigm for decision making between alternative cell fates during development (Court et al., 2007; St-Pierre and Endy, 2008). During the decision process, the regulatory circuit encoded by viral genes (primarily *cI*, *cII*, and *cro*) integrates multiple physiological and environmental signals, including the number of infecting viruses and the metabolic state of the cell, in order to reach a decision (Weitz et al., 2008). More than a decade ago, Arkin and coworkers (Arkin et al., 1998) used a numerical study of the lambda lysis/lysogeny decision following infection to emphasize the role of stochasticity in genetic circuits. Their work led to the emergence of the widely accepted picture of cell variability driven by spontaneous biochemical stochasticity, not only in lambda (Arkin et al., 1998; Singh and Weinberger, 2009) but in other systems as well (Chang et al., 2008; Losick and Desplan, 2008; Maamar et al., 2007; Singh and Weinberger, 2009; Suel et al., 2007). More recently, however, it was shown by St-Pierre and Endy that, at the single-cell level, cell size is correlated with cell fate following lambda infection, thus explaining away some of the observed cell-fate heterogeneity and reducing, though not eliminating, the expected role of biochemical stochasticity in the decision (St-Pierre and Endy, 2008).

For the purpose of deconstructing the lambda postinfection decision, a few candidates should be considered as possible hidden microscopic parameters affecting cell fate. The number of phages infecting an individual cell (multiplicity of infection; MOI) has long been known to affect cell fate (Kourilsky and Knapp, 1974), although the quantitative form of this dependence has been unclear (Kourilsky and Knapp, 1974). In addition, recent results suggest that both the volume of the infected cell (St-Pierre and Endy, 2008) and the position of the infecting phages on the cell surface (Edgar et al., 2008) may be important. Some or all of these parameters are hidden from us, not only in bulk experiments but also in single-cell assays where the individual infecting viruses cannot be tracked (St-Pierre and Endy, 2008). We thus set out to examine the infection process at the level of individual phages and cells at a spatiotemporal resolution sufficient to quantify the relevant subcellular parameters. This allowed us, in turn, to evaluate the contribution of each factor to the observed cell-fate heterogeneity.

RESULTS

Assaying the Postinfection Decision with Single-Phage Resolution

To enable detection of individual phages, we constructed a fluorescently labeled lambda strain (λ_{LZ2}; for details, see the Experimental Procedures). The phage capsid contains a mixture of the wild-type head-stabilization protein gpD and a fusion protein of gpD and yellow fluorescent protein (EYFP), gpD-EYFP (Alvarez et al., 2007). These "mosaic-YFP" phages were detectable as diffraction-limited objects under epifluorescent illumination (Figure 1A). The presence of fluorescent proteins in the viral capsids did not perturb the phage phenotype: the phages exhibited normal capsid morphology (see Figure S1 available online); they packed viral DNA at close to 100% efficiency (Figure 1A); and, most importantly, their lysogenization phenotype, as measured in bulk, was indistinguishable from that of wild-type phages (Figure S1).

To characterize the postinfection decision, individual infection events were followed under the fluorescence microscope (Figure 1; see also the Experimental Procedures and Movie S1). The initial infection parameters were recorded: the number and positions of phages infecting each individual cell, as well as the size of the infected cell. Time-lapse microscopy was then used to examine the fate of each infected cell. Choice of the lytic pathway was evinced by the production of many new fluorescent phages, followed by cell lysis (Figures 1B and 1C). Lysogeny was detected through a transcriptional reporter plasmid expressing mCherry from the P_{RE} promoter, which controls the establishment of lysogeny (Kobiler et al., 2005) (Figures 1B and 1C). The majority of infected cells (75%, 1048/1394 cells, 22 experiments) exhibited either lysis or lysogeny following infection. A small fraction of the infection events (10%, 143/1394 cells) did not lead to either lysis or lysogeny, and cells resumed normal growth. Examination of the failure frequency as a function of MOI (Figure 2A) suggested a failure probability per phage of 23% ± 2% (SEM, 104/446 events). This value is in good agreement with previous bulk estimates (Mackay and Bode, 1976). Failed infections are likely the result of failed (or incomplete) injection of viral DNA into the cell (Mackay and Bode, 1976). Another subpopulation (15%, 203/1394 cells) exhibited a halting of cell growth following infection. This phenomenon, previously reported in the literature (Koster et al., 2009; Kourilsky, 1973), exhibited a sharp threshold dependence on MOI (Figure 2B), with the fraction of nongrowing cells rising from 6.5% (29/446 cells) at MOI = 1 to 81% (48/59 cells) at MOI $\geq$ 10. As additional evidence for the fidelity of our infection assay, we observed that infection of cells that have already been lysogenized, and which should be immune to further infections (Hershey, 1971), indeed resulted in 0% lytic development (0/43 cells; Figure 2C). On the other hand, infection at 40°C, where the repressor proteins produced by the phages are inactivated (Hecht et al., 1983; Hershey, 1971), led to 100% lysis (50/50 cells; Figure 2C).

Infection Parameters Affecting Cell Fate

We next examined the effect of different infection parameters on the resulting cell fate (among cells undergoing lysis or lysogeny; Figure 2). In agreement with previous bulk experiments (Kourilsky and Knapp, 1974), the probability of lysogeny f increased with the number of phages m infecting an individual cell (MOI) (Figure 2C). The probability f approached ~1 (100% lysogeny) when m was sufficiently large. To characterize the imprecision (or noisiness) of the observed decision, we fit $f(m)$ to a Hill function (Alon, 2007), $f(m) = m^h/(m^h+K^h)$. The Hill coefficient h can then be used as a phenomenological indicator for the decision precision: the range of input parameters Δm for which both fates can be observed is proportional to $1/h$ (see the Experimental Procedures). Thus, the higher h, the higher the chance of observing a unique cell fate (less cell-fate heterogeneity is observed), and the decision can be said to be more precise (less noisy). For $f(m)$, we find $h \approx 1$ (h = 1.00 ± 0.10 [SEM],

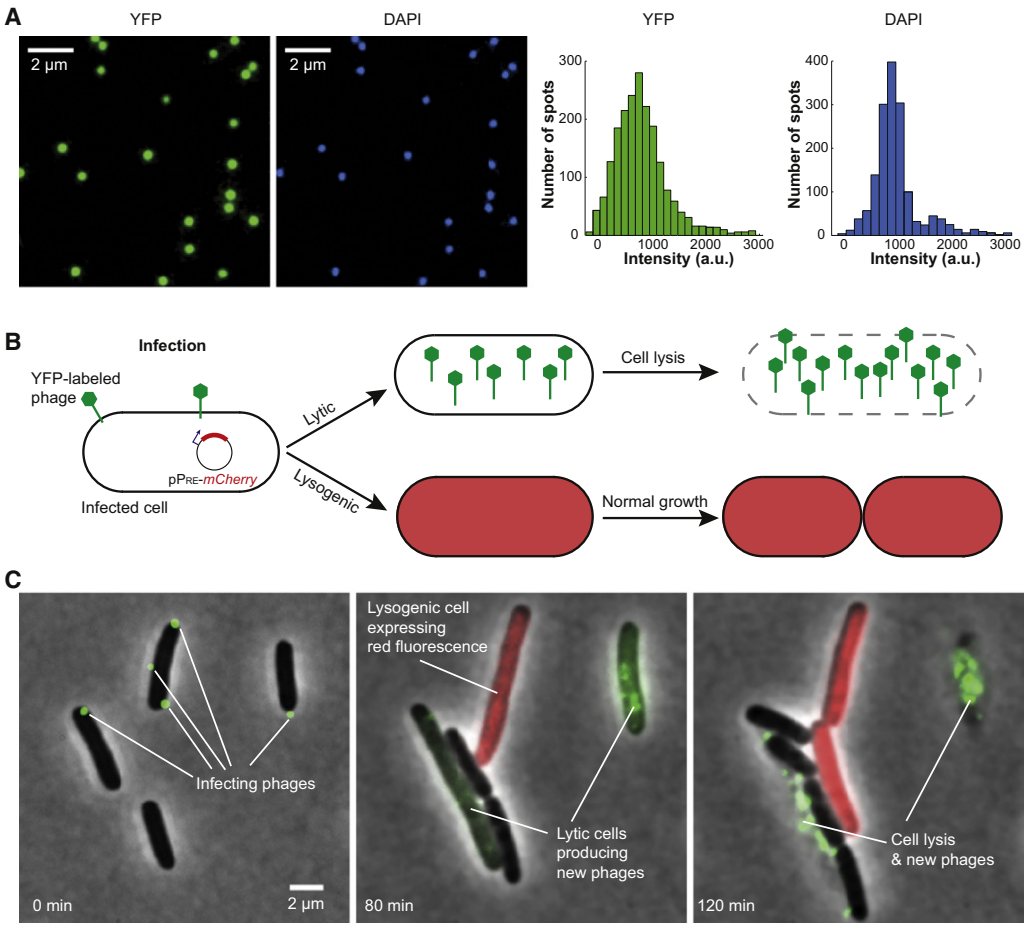

Figure 1. Assaying the Postinfection Decision with Single-Phage Resolution

(A) Fluorescence and DNA packaging efficiency of the gpD-mosaic phage (λ_{LZ2}). DAPI (4′,6-diamidino-2-phenylindole) was used to label the phage genome. Left two panels: YFP and DAPI signals from the phages under the fluorescence microscope. YFP and DAPI signals colocalize very well, and individual phages are easily distinguishable. Only ~1% of the gpD-mosaic phage particles examined (12 out of 1080) lacked the DAPI signal (indicating that these particles did not successfully package the viral DNA or had already injected their DNA elsewhere). On the other hand, all the phage particles (1068 out of 1068) were well labeled by YFP, as each DAPI spot had a corresponding YFP spot. Right two panels: intensity histograms of the YFP and DAPI signals.

(B) A schematic description of our cell-fate assay. Multiple YFP-labeled phages simultaneously infect individual cells of *E. coli*. The postinfection fate can be detected in each infected cell. Choice of the lytic pathway is indicated by the intracellular production of new YFP-coated phages, followed by cell lysis. Choice of the lysogenic pathway is indicated by the production of mCherry from the P_{RE} promoter, followed by resumed growth and cell division. The three stages of the process correspond to the three images seen in (C) below.

(C) Frames from a time-lapse movie depicting infection events (see also Movie S1). Shown is an overlay of the phase-contrast, mCherry, and YFP channels (YFP channel: sum of multiple z slices for t = 0; single z slice at later time frames). At t = 0 (left), two cells are seen each infected by a single phage (green spots), and one cell is infected by three phages. At t = 80 min (middle), the two cells infected by single phages have each gone into the lytic pathway, as indicated by the intracellular production of new phages (green). The cell infected by three phages has gone into the lysogenic pathway, as indicated by the production of mCherry from the P_{RE} promoter (red). At t = 2 hr (right), the lytic pathway has resulted in cell lysis, whereas the lysogenic cell has divided. (Note: a number of unadsorbed phages were removed from the image for clarity; those can be seen in Movie S1.)

See also Figure S1, Table S1, and Movie S1.

1706 cells). As we show below, characterizing the lysogeny decision at the level of individual infecting phages reveals a much sharper (less noisy) decision. Integrating over the decisions of individual phages infecting the same cell allows us, in turn, to reproduce the observed whole-cell phenotype.

Another factor affecting the decision is the length of the infected cell (which serves as a metric for both its age [Neidhardt et al., 1990] and its volume). As seen in Figure 2C, for a given m, shorter cells exhibited a higher propensity to lysogenize. This result complements previous results obtained at $m = 1$, in which cell fate was shown to be correlated with cell volume (St-Pierre and Endy, 2008). As for the position of the infecting phages, we observed that infecting phages preferentially attached to the cell pole and midcell, in agreement with recently reported results (Edgar et al., 2008) (Figure 2D). Imaging performed at high temporal resolution for short durations revealed that adsorbed phages diffuse on the cell surface for the first few seconds of the adsorption process, but then become practically

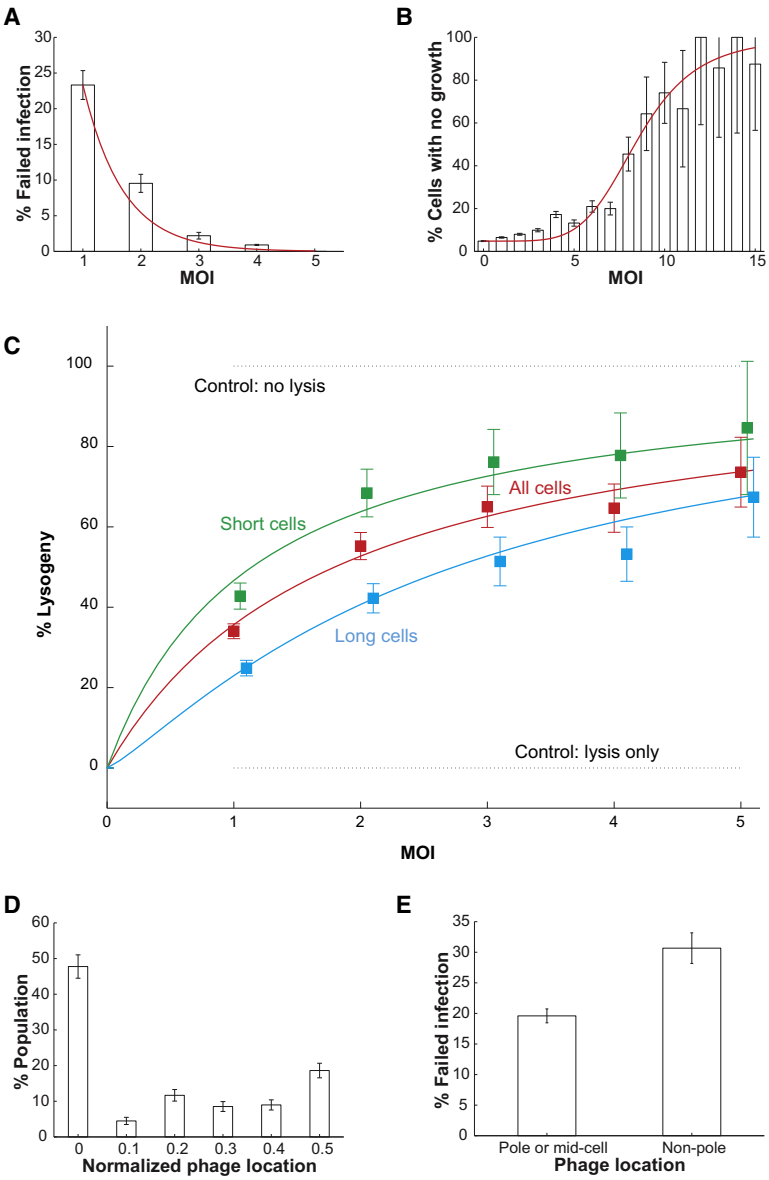

Figure 2. Infection Parameters Affecting Cell Fate

(A) The percentage of failed infections as a function of multiplicity of infection (MOI). Red line: fit to an exponent, suggesting a constant failure probability per phage.

(B) The percentage of nongrowing cells as a function of MOI. Red line: fit to a Hill function, suggesting a threshold response to the number of infecting phages.

(C) The percentage of cells undergoing lysogeny, as a function of the MOI. Filled squares: experimental data. Solid line: fit to a Hill function. Red: all cells (1706 cells). Blue: long cells (length ≥ population median, 879 cells). Green: short cells (length < population median, 827 cells). The lysogeny probability increases with MOI, and is higher for shorter cells compared to longer ones. Also shown (dotted lines) are control experiments yielding lysis only (infection at 40°C; bottom) or no lysis (infection of lysogens; top).

(D) Distribution of infecting phage position along the cell, for MOI = 1. Distance is measured from cell pole (0) to midcell (0.5). Approximately 66% of all phages infect at either the pole or midcell (future pole).

(E) The percentage of failed infections as a function of infecting phage position, for MOI = 1. Infections at the pole and midcell are less likely to fail than infections at other positions (20% versus 31%, p = 0.041).

In all plots, error bars denote standard error of the mean. Data are represented as mean ± SEM.

immobilized, with a position fixed to within ~100 nm (data not shown). The position of the infecting phage did not seem to affect the choice between lysis and lysogeny (at MOI = 1, 33% ± 2% [SEM] lysogeny for polar infections versus 37% ± 4% [SEM] for nonpolar infections, 71/213 versus 37/100). However, the importance of the infection site was revealed when examining the probability of failed infection (Figure 2E). Infections at the cell pole and midcell were less likely to fail than infections at other parts of the cell (20% ± 1% versus 31% ± 3% [SEM] failure rate, 58/296 versus 46/150 cells). Thus, when considering the probability of failed infection (in addition to lysis and lysogeny), the position of infecting phages did affect the final outcome of infection, with a higher chance of lysogenization for phages infecting the poles. For $m = 2$, an infection by two phages at the cell poles yielded 29% more lysogens than infections by two nonpolar phages (68/108 versus 18/37). The dependence of infection success on position could be the result of the localization of key proteins required for successful DNA injection, such as ManY, at the poles and midcell (Edgar et al., 2008).

Lysogeny Requires a Unanimous Decision by All Infecting Phages

Previous studies (St-Pierre and Endy, 2008; Weitz et al., 2008) have suggested that the relevant parameter affecting cell fate is not the absolute number of infecting phages m but rather the "viral concentration" m/V, where V is the cell volume. This suggestion is based on the observation that m/V determines the dosage of viral-encoded genes, which in turn governs the postinfection decision (Weitz et al., 2008). To examine this hypothesis, we mapped the dependence of f on both cell length l (a proxy for cell volume) and multiplicity-of-infection m (Figure 3). If the viral-concentration hypothesis is correct, then $f(m,l)$ should be a function of m/l only. Thus, for example, the chance of lysogenization will be the same for a single phage infecting a cell of length l_0 as for two phages infecting a cell of length $2l_0$. As seen in Figure 3B, however, this is not the case. When plotting f versus m/l, the f values for different ms do not fall on the same line. Specifically, the curves become flatter for higher MOIs. To explain this behavior, we note that the (m/l) scaling is based on the assumption of a single decision made at the whole-cell level. The possibility of an earlier "subcellular" step, namely that of an independent (possibly noisy) decision by each infecting phage, is not included. To incorporate this feature, we examined the following hypothesis: when m phages infect a cell, each phage independently chooses between lysis and

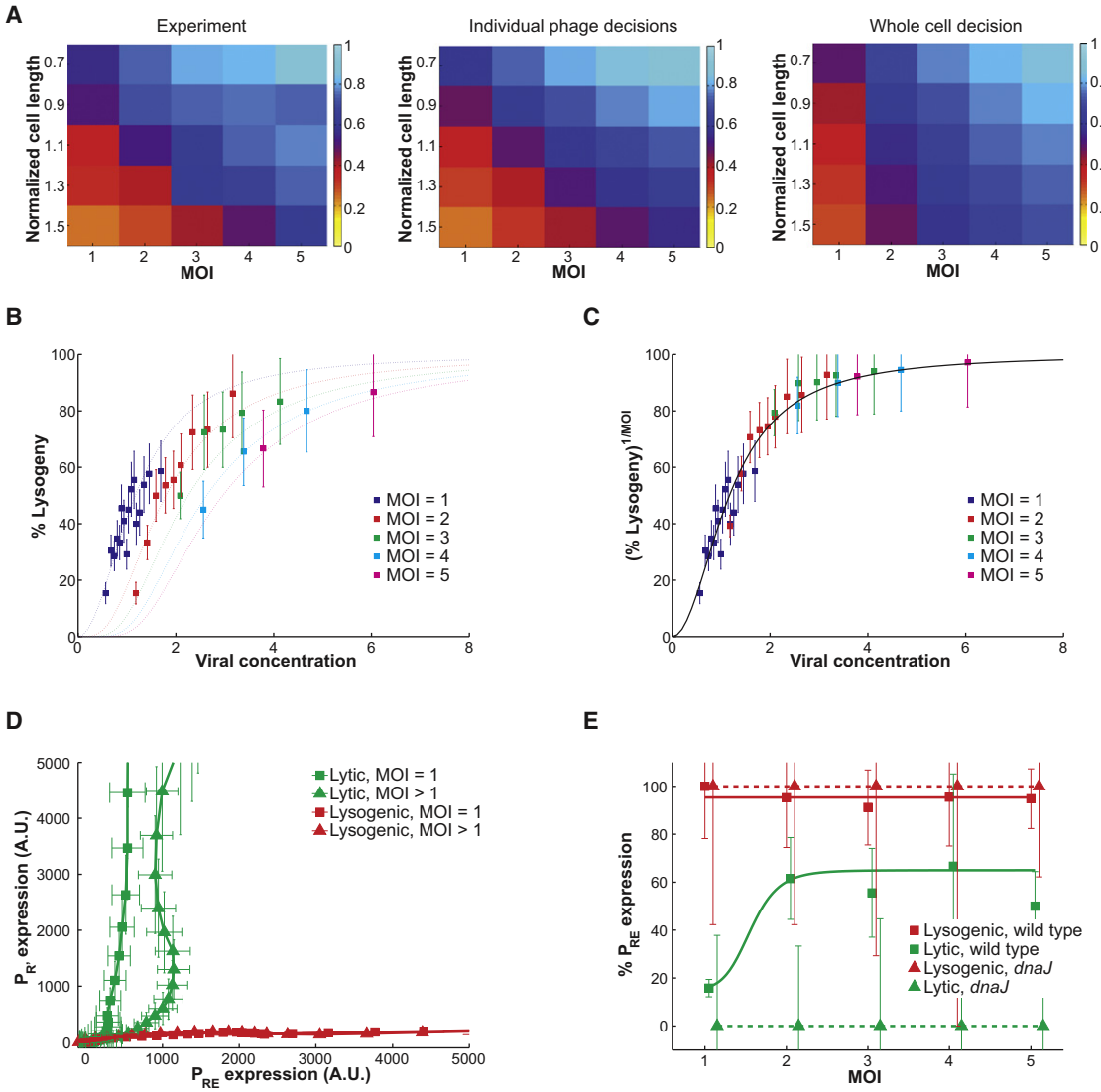

Figure 3. Lysogeny Requires a Unanimous Decision by All Infecting Phages

(A) Two-dimensional color map depicting the probability of lysogeny as a function of MOI and normalized cell length (length divided by the population median). Left: experimental data (1072 cells). Center: theoretical model assuming that a unanimous decision by all phages is required for lysogeny. This model predicts $f(m,l) = [f_1(m/l)]^m$, where m = MOI and l = normalized cell length. $f_1(m/l)$ is derived from the data scaling observed in (C). Note the good agreement between theory and experiment. Right: theoretical model assuming a single decision at the whole-cell level, with $f(m,l) = f(m/l)$. $f(m/l)$ is derived from fitting the data in (B) to a single curve. Note that this model does much more poorly than the phage-decision model in capturing the topography of $f(m,l)$, for example the position of the $f = 0.5$ contour line.

(B) Probability of lysogeny f as a function of viral concentration (m/l). The data from different MOIs (filled squares, different colors) do not collapse into a single curve, but instead can be fitted to the separate curves $f(m,l)$ described in (A) (dotted lines).

(C) Scaled probability of lysogeny ($[f(m,l)]^{1/m}$) as a function of viral concentration (m/l). Data from different MOIs (filled squares, different colors) collapse into a single curve, representing the probability of lysogeny for each individual infecting phage (f_1), in a cell of length l infected by a total of m phages. f_1 can be fitted to a Hill function, $f_1(m/l) = (m/l)^h/(K^h+(m/l)^h)$, with $h = 2.07 \pm 0.11$, $K = 1.17 \pm 0.02$ (SEM).

(D) Gene-expression trajectories of different cell populations following infection. Each line describes the average expression level of P_{RE} and $P_{R'}$ during the first 60 min after infection. Green squares, lytic cells, MOI = 1 (average of 19 cells). Red squares, lysogenic cells, MOI = 1 (average of 21 cells). Green triangles, lytic cells, MOI > 1 (average of 37 cells). Red triangles, lysogenic cells, MOI > 1 (average of 135 cells). As predicted by the phage-voting hypothesis, cells choosing lysis after infection by MOI > 1 phages exhibit on average an increased activity of P_{RE}, suggesting a "mixed voting" inside the cell.

(E) Percentage of cells expressing the lysogeny promoter P_{RE}, as a function of the number of infecting phages (MOI). Green squares, lytic cells, wild-type (total of 56 cells). Red squares, lysogenic cells, wild-type (total of 156 cells). Green triangles, lytic cells, *dnaJ* host (total of 34 cells). Red triangles, lysogenic cells, *dnaJ* host (total of 16 cells). Lines are a guide for the eye. When infecting a wild-type host, the fraction of lytic cells expressing P_{RE} rises sharply at MOI > 1, suggesting a mixed voting inside the cell. When infecting a *dnaJ* host, the voting rule changes such that even a single phage choosing lysogeny leads to whole-cell lysogeny. In that case, no mixed voting is seen among cells choosing lysis. Cells choosing lysogeny express P_{RE} at all MOIs in both hosts. Data are represented as mean ± SEM.

lysogeny. The probability of an individual phage choosing the lysogenic pathway (denoted f_1) depends on the viral concentration alone, and is thus given by $f_1 = f_1(m/l)$. There is still a finite probability ($1 - f_1$) that the phage will choose the lytic pathway. The expression of lytic genes from a single phage will in turn activate the lytic pathway response in the whole cell, since this pathway is the default state of the lysis/lysogeny switch (Court et al., 2007; Oppenheim et al., 2005). In contrast, for the lysogenic pathway to be chosen in the cell, all m phages have to choose lysogeny, an event that will happen with a probability $[f_1]^m$. We therefore expect, for a cell infected by m phages, that $f(m,l) = [f_1(m/l)]^m$. As seen in Figure 3C, this turns out to be the case. Plotting $[f(m,l)]^{(1/m)}$ versus (m/l) collapses the data from different MOIs into one curve.

The functional form revealed by Figure 3C, $f(m,l) = [f_1(m/l)]^m$, should be understood as follows: $f_1(m/l)$ is the probability of an individual phage choosing lysogeny, given that a cell of length l has been infected by m phages. This function is sigmoidal in (m/l), reflecting the fact that, for each infecting phage, the probability of lysogenization increases sharply with the viral concentration inside the cell. Note that, compared to the single-cell response $f(m)$, the single-phage "decision curve" displays a sharper threshold behavior, i.e., is less noisy. When fitted to a Hill function, the Hill coefficient obtained is $h = 2.07 \pm 0.11$ (SEM) (compared to $h = 1.0 \pm 0.10$ [SEM] observed at the whole-cell level). This threshold behavior obviously could not have been unveiled were our measurements limited to the resolution of individual cells but not individual viruses. The whole-cell lysogenization probability $f(m,l)$ scales like the single-phage probability $f_1(m/l)$ to the power m. This scaling indicates that only if all m phages infecting a cell choose lysogeny is that fate followed. Thus, once each phage has made its (noisy) decision, a precise (noiseless) cellular decision is made based on those individual-phage votes. The logic of the cellular decision can be thought of as a simple "AND" gate, such that only if all inputs are "1" (i.e., lysogeny) will this be the cellular output (see below).

The quality of the agreement between the individual-phage-decision hypothesis and experiment is further demonstrated in Figure 3A. For comparison, we plot the predicted $f(m,l)$ map for two different hypotheses: (1) $f(m,l) = [f_1(m/l)]^m$, i.e., decisions by the individual phages, followed by the requirement for a unanimous vote to establish lysogeny; and (2) $f(m,l) = f(m/l)$, i.e., a single decision at the whole-cell level, based on the viral concentration inside the cell. As can be seen, only the former scenario is able to capture the essential topography of the $f(m,l)$ map. The superior agreement between theory and experiment is also evident in the quality of the curve fit (sum of squared error): a value of 0.10 for the phage-decision hypothesis versus 0.30 for the whole-cell decision.

To further test our hypothesis regarding the decision mechanism, we note that the requirement for a unanimous phage vote to obtain lysogeny has the following consequence: among cells infected by $m > 1$ phages and choosing lysis, there should be a subpopulation in which some of the infecting phages actually chose lysogeny, but that decision was "overruled" by the presence of other phages in the cell choosing lysis. To test for this scenario of "mixed voting," we used our fluorescence reporters described above to assay the activity of the lysogeny-establishment promoter (P_{RE}, expressing mCherry), as well as the late lytic promoter ($P_{R'}$, expressing gpD-EYFP) in individual cells following infection. As can be seen in Figure 3D, gene activity of cells undergoing lysis supports the "mixed-voting" prediction: the average trajectory taken by lytic cells infected by a single phage is "strictly lytic"; no significant activity of P_{RE} is detected in these cells. On the other hand, lytic cells at $m > 1$ show, on average, increased activity of P_{RE} before committing to lysis. As an additional control, it can be seen that lysogenic cells do not exhibit significant late-promoter activity at either $m = 1$ or $m > 1$, consistent with our observation that lysogeny requires that all infecting phages choose lysogeny. To further quantify this "mixed-voting" phenotype, we measured the fraction of lytic cells displaying P_{RE} activity as a function of the number of infecting phages m (Figure 3E). As expected, this fraction increases sharply for $m > 1$. For comparison, the fraction of lysogenic cells displaying P_{RE} activity is close to 100% at all values of m, as expected.

We next asked whether the "voting rule," which gives lysogeny only if all phages choose that fate, can be modified by "handicapping" the lytic pathway. The rationale was the following: the unanimous vote required for lysogeny means that lysis is the default route, and will always be chosen unless a cell is forced otherwise. Altering this behavior requires tilting the balance between lysis and lysogeny, which could possibly be achieved by partially inhibiting the lytic pathway. In *dnaJ* mutants of *E. coli*, lambda replication is severely inhibited (Sunshine et al., 1977; Yochem et al., 1978), and the lytic pathway is believed to begin but not reach completion (Sunshine et al., 1977; Yochem et al., 1978). There is no evidence that the decision-making circuit is affected by this host mutation, and thus according to the standard picture the cellular decision phenotype should not change. However, in light of our observation of intracellular voting, we hypothesized that in a *dnaJ* host the lytic pathway will lose its built-in advantage over lysogeny; as a result, it is possible that the requirement for a unanimous vote for achieving lysogeny will be lifted, and thus even a single phage choosing lysogeny may result in cell lysogeny rather than lysis. In that case, lytic cells would not be expected to exhibit a "mixed-vote" phenotype but a uniform "lysis-only" gene activity. As can be seen in Figure 3E, this is indeed the case. *dnaJ* cells undergoing lysis did not exhibit P_{RE} activity, in contrast to the behavior of the wild-type host described above. In other words, a different voting rule is used to reach the lysis/lysogeny decision in the *dnaJ* host.

The Precision of the Single-Phage Decision Is Lost at the Single-Cell Level

As an additional test for the validity of our results regarding the decision hierarchy in the cell, we next reversed the process and attempted to reconstruct the observed decision-making phenotype at the level of the whole cell and the whole population, starting from the single-phage response curve found above (Figure 4; see also the Experimental Procedures). This was done by integrating over the different degrees of freedom that remain hidden in the lower-resolution (coarse-grained) experiments. Thus, when going from individual phages to the whole cell, we began with $f_1(m/l)$ (Figure 4A) and integrated over the

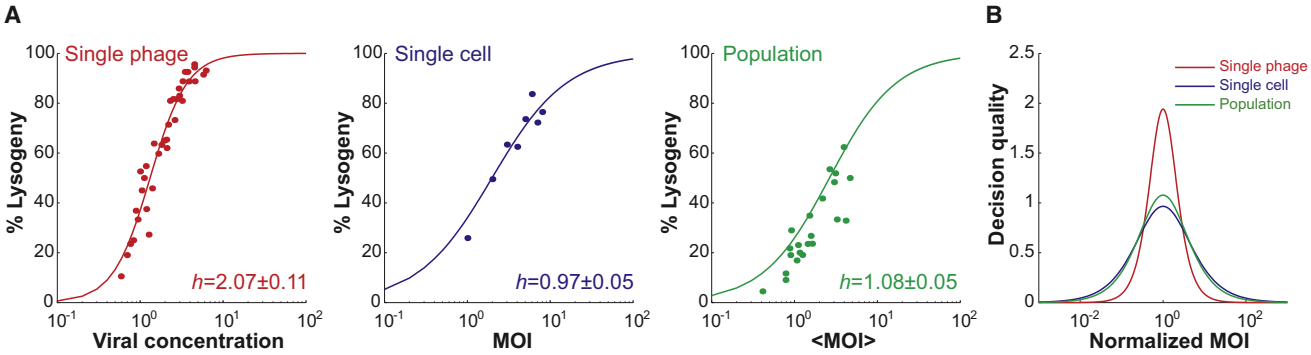

Figure 4. The Precision of the Single-Phage Decision Is Lost at the Single-Cell Level

(A) The probability of lysogeny as a function of the relevant input parameter, at the single-phage (left, red; input is viral concentration m/l), single-cell (middle, blue; input is MOI of the individual cell), and population-average (right, green; input is the average MOI over all cells) levels. Circles: experimental data. Solid lines: theoretical prediction, fitted to a Hill function. The decision becomes more "noisy" (lower Hill coefficient) when moving from the single-phage to the single-cell level. Moving from the single cell to the population average does not decrease the Hill coefficient further.

(B) The same trend can be observed by plotting the "response function" $R(x) = \partial f(x)/\partial(\log(x))$ at each resolution level. $R(x)$ describes the range of input parameters x where both cell fates coexist (and therefore the decision can be said to be noisy). Single-cell and population experiments exhibit similar forms of $R(x)$, significantly broader than that observed for individual phages. All curves are derived from the theoretical values in (A).

See also Figure S2.

spatial positions of phage infections and their effect on infection efficiency, as well as the length distribution of cells in the population (Figure S2), obtaining the predicted single-cell MOI response curve, $f(m)$. We then integrated further over the random phage-bacterium collision probabilities (Moldovan et al., 2007) to obtain the predicted population-averaged MOI response, $f(M)$. We found that the predicted decision curves agree well with the experimental ones (Figure 4A), demonstrating that we have successfully deconstructed the sources of observed noise in the single-cell and population-averaged response. Notably, when comparing the decision curves at the different resolution levels (Figure 4B), one observes that most of the apparent noise in the decision arises at the transition from the single-phage to the single-cell level, when integrating over individual-phage decisions and the distribution of cell ages in the population. Below we discuss the reasons for the accumulation of "phenotypic noise" at the single-cell level. Moving further from individual cells to the population average did not add significantly to the observed imprecision of the decision.

DISCUSSION

In recent years, single-cell experiments have often been used to unveil the heterogeneity of cell-fate decisions and to elucidate the origins of this heterogeneity (Blake et al., 2003, 2006; Kærn et al., 2005; Locke and Elowitz, 2009; Longo and Hasty, 2006; Muzzey and van Oudenaarden, 2009). Specifically, the inherent stochasticity of gene expression has been hypothesized (Arkin et al., 1998; Singh and Weinberger, 2009) and demonstrated (Maamar et al., 2007; Suel et al., 2007) to be an important source of cell-fate heterogeneity. More recently, however, it has been shown that higher-resolution measurements of cellular parameters can unveil "hidden variables" that have a deterministic effect on cell fate. Thus, the role played by true chemical stochasticity may be smaller than previously thought. The work presented here furthers the observation that examining decision making at the level of individual cells is not always sufficient for unveiling the true sources of cell-fate heterogeneity. In particular, we found that in the case of lambda postinfection decision, measurements at the single-cell level mask as much of the critical degrees of freedom as measurements made in bulk (see Figure 4)—counter to the widely accepted view of this system (Arkin et al., 1998; Singh and Weinberger, 2009).

The reason for the inadequacy of single-cell resolution is that the cell-fate decision is achieved through a hierarchy of decisions at the subcellular level. A choice between lysis and lysogeny is first taken at the level of individual viruses infecting the cell. Each infecting virus makes a decision in favor of lysis or lysogeny, with the probability of lysogeny dependent on the concentration of viral genomes in the infected cell. Next, a cellular decision is reached based—in a precise manner—on the decisions of all individual phages (Figure 5). Only if all viruses infecting a single cell vote in favor of lysogeny is that fate chosen; otherwise, the lytic pathway ensues. We note that the two-step decision process renders the whole-cell phenotype noisy, in the sense that for a broad range of multiplicity-of-infection values m, both cell fates can be observed (recall that $f(m)$ has a Hill coefficient ≈ 1; Figure 4 above). The enhancement of phenotypic noise in the transition from single phage to single cell is largely the result of the following competition effect: on one hand, the probability that an individual phage will choose lysogeny rises sharply as a function of m ($f_1(m/l)$ has a Hill coefficient ≈ 2; Figure 4). On the other hand, the higher the m, the smaller the chance that *all* phages infecting the cell will vote the same way and allow cell lysogeny (recall that $f(m,l)$ scales like the single-phage probability $f_1(m/l)$ to the power m). Thus, the sharp single-phage response, combined with the "AND" gate that follows, result in a "smeared" decision curve at the whole-cell level.

We also note that the threshold response observed in the single-phage lysogenization probability f_1, as a function of the

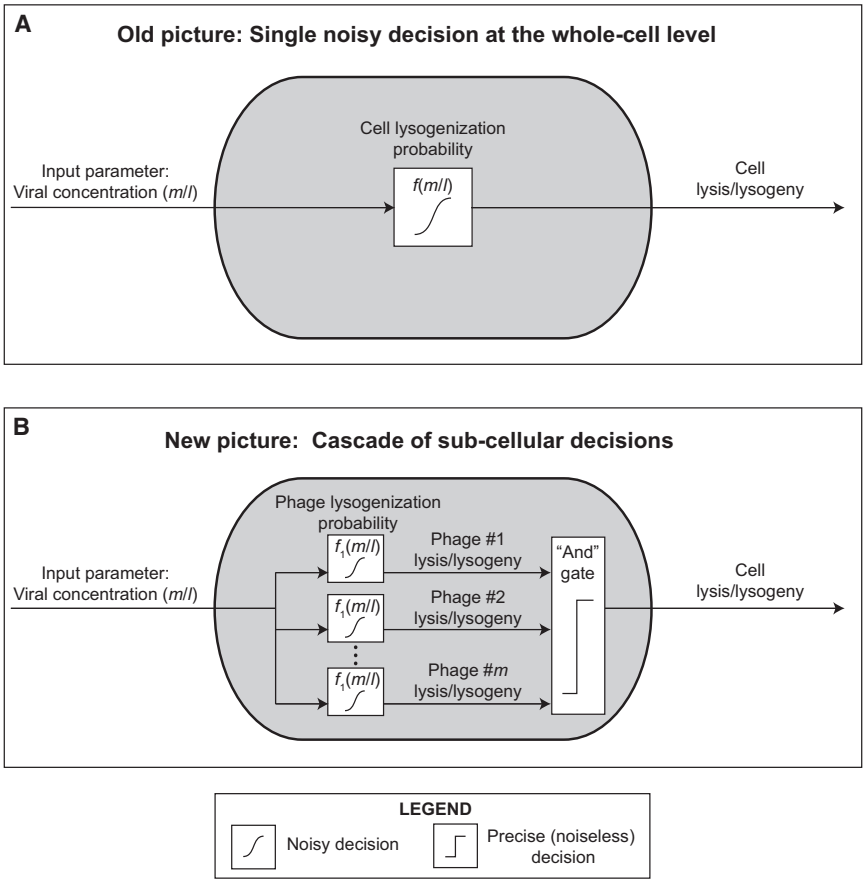

Figure 5. Hierarchical Decision Making Determines Cell Fate following Lambda Infection

(A) The traditional description of the postinfection decision consists of a single noisy decision at the whole-cell level. When m phages infect a cell of size l, the viral concentration (m/l) serves as an input parameter to the cell-fate decision (St-Pierre and Endy, 2008; Weitz et al., 2008). The outcome is lysis or lysogeny, with the lysogeny probability given by $f(m/l)$. $f(m/l)$ is very noisy ($h \approx 1$; see Figure 4 above), and the noise is attributed to biochemical stochasticity (Arkin et al., 1998; Singh and Weinberger, 2009).

(B) Decision making at the subcellular level: according to the results presented in this work, cell fate is obtained through a two-step decision process. When m phages infect a cell of size l, the viral concentration (m/l) serves as an input parameter to the lysis/lysogeny choice by each individual phage. The lysogeny probability $f_1(m/l)$ exhibits a sharp threshold response to the viral concentration ($h \approx 2$; see Figure 4 above), but is still noisy enough to allow lysis to be chosen. The choices of all infecting phages are then integrated through a logical "AND" gate, such that only if all phages choose lysogeny is that pathway pursued.

viral concentration (m/l), is in agreement with the prediction of a simple theoretical model of the gene regulatory circuit governing the decision (Weitz et al., 2008). When writing a deterministic description of the kinetics of CI, CII, and Cro, the threshold-crossing behavior emerges naturally, and does not require invoking any stochasticity (Weitz et al., 2008). In our measurements, we did not observe a "perfect" threshold (a step function, corresponding to an infinite Hill coefficient), but a "smooth" one ($h \approx 2$). Further studies are required in order to determine whether the observed deviation from a noiseless single-phage decision is fully explained by the inherent stochasticity of gene activity in the system.

The concept of decision making at the subcellular level may at first appear counterintuitive: presumably, all of the relevant regulatory proteins produced from the individual viral genomes (e.g., CI, CII, and Cro) achieve perfect mixing in the bacterial cytoplasm within seconds of their production, due to diffusion (Elowitz et al., 1999). How then is viral individuality inside the cell maintained? The answer may lie in the discreteness of viral genomes and of the gene-expression events underlying the decision-making process. In the lambda case, a lytic choice by a single phage will be manifested by the cascade of transcription and antitermination events along a single viral genome (Court et al., 2007; Oppenheim et al., 2005), resulting in the bursty expression (Cai et al., 2006; Golding et al., 2005; Yu et al., 2006) of lytic genes. This in turn will activate the lytic pathway response in the whole cell, which is characterized by a trigger response to the lytic protein Q (Kobiler et al., 2005). Thus, a subcellular single-genome event may serve as a "singular perturbation" (Goldenfeld, 1992), which then gets amplified to the whole-cell level. The scenario described above bears some resemblance to the amplification of a single gene-expression event into a cellular phenotypic switching, recently suggested in the lactose system (Choi et al., 2008).

In addition, despite the commonly made assumption of "perfect mixing" in bacterial cytoplasmic reactions, we cannot rule out the possibility that subcellular decision making is enabled by spatial separation of key players in the process. Nonhomogeneous spatial patterns of bacterial proteins (Thanbichler and Shapiro, 2008), RNA (Russell and Keiler, 2009), and DNA (Sherratt, 2003; Thanbichler and Shapiro, 2008) have been demonstrated. Specifically, *E. coli* proteins ManY and FtsH, believed to be involved with the lambda lysis/lysogeny decision, were found to be localized to the cell pole (Edgar et al., 2008). In another recent work, replicating Φ29 phage genomes were shown to interact with the host-encoded MreB proteins, forming a helix-like pattern near the membrane of infected *B. subtilis* cells (Munoz-Espin et al., 2009). Further studies, possibly at spatial resolution beyond that afforded by diffraction-limited microscopy (Huang et al., 2009; Lippincott-Schwartz and Patterson, 2009), will be needed to elucidate the possible role of spatial compartmentalization in yielding a discrete single-phage decision in the lambda system.

Beyond the simple bacteriophage system investigated here, it is intriguing to contemplate the possibility of subcellular decision

making at the other end of the complexity spectrum, in higher eukaryotic systems. In those systems, multiple copies of a gene circuit often exist, and copy-number variations play a critical role in health and disease (Cohen, 2007). The question then arises, would individual gene copies in the cell exhibit independent decisions, as the phage genomes do? In addition, intracellular compartmentalization is of course well established in higher cells (Alberts, 2009). However, how this spatial organization affects the process of cell-fate determination is largely unexplored. We believe that elucidating the possible relation between intracellular spatial organization and cell-fate decisions promises to be a rewarding area of research.

EXPERIMENTAL PROCEDURES

A more detailed description of materials and methods can be found in the Extended Experimental Procedures.

Preparation of the gpD-Mosaic Phage

We constructed a gpD-mosaic phage, inspired by previous work (Zanghi et al., 2005), showing stable phage assembly when wild-type and recombinant versions of gpD capsid proteins were coexpressed. First, a gpD-EYFP phage, λ_{LZ1}, was obtained by crossing λeyfp [*cI857 Sam7 D-eyfp*] (Alvarez et al., 2007) (gift of Philippe Thomen, Université Pierre et Marie Curie) with plasmid pJWL464 (Michalowski et al., 2004) (gift of John Little, University of Arizona), resulting in a *kanR* cassette inserted into λ *b* region (λ coordinates 5′-23901–26818-3′), which is considered nonessential (Hendrix, 1983). We also constructed pPLate*D*, containing the λ *D* gene under the control of the λ late promoter. To create the gpD-mosaic phage, an overnight culture of LE392(λ_{LZ1}) [pPLate*D*] was grown in LB in the presence of appropriate antibiotics. The culture was diluted 1:100 into LBM (LB supplemented with 10 mM $MgSO_4$) and grown at 30°C with mild shaking (180 rpm) to $OD_{600} \approx 0.6$. The lysogen culture was induced by increasing the temperature to 42°C for 18 min, and then incubated at 37°C with mild shaking until lysis was visible (culture became clear). Purified phage was prepared based on standard protocols (Sambrook and Russell, 2001).

Single-Cell Infection Assay

An overnight culture of LE392[pP_{RE}-*mCherry*] was diluted 1:1000 in LBMM (LB supplemented with 10 mM $MgSO_4$ and 0.2% maltose) supplemented with appropriate antibiotics and grown to $OD_{600} \approx 0.4$. Cells were concentrated and resuspended in ice-cold LBMM to $OD_{600} \approx 20$. λ_{LZ2} phages were added to reach an MOI of 0.1–5, followed by incubation on ice for 30 min and an additional 5 min incubation at 35°C to trigger phage DNA injection (Edgar et al., 2008; Kourilsky, 1973; Mackay and Bode, 1976). One microliter of the phage-cell mixture was diluted 1:10 into LBMM at room temperature and placed on a thin 1.5% LBM (LB supplemented with 10 mM $MgSO_4$) agarose slab (~1 mm thick). After 1 min, a coverslip (no. 1; Fisher Scientific) was gently overlaid and the sample was imaged under the fluorescence microscope at room temperature. Microscopy was performed on an inverted epifluorescence microscope (Eclipse TE2000-E; Nikon) using a 100× objective (Plan Fluor, numerical aperture 1.40, oil immersion) and standard filter sets. Images were acquired using a cooled CCD camera (Cascade512; Photometrics). Acquisition was performed using MetaMorph software (Molecular Devices).

To localize all phages surrounding the cells, a series of 15 z axis (vertical) images at a spacing of 200 nm was taken through the YFP channel using a 1000 ms exposure for each. To obtain more data in each time-lapse movie, cells were imaged at multiple stage positions (typically 8) in each experiment. During the time-lapse movie, the sample was imaged in phase contrast (100 ms exposure, for cell recognition), YFP (400 ms exposure, for phage detection), and mCherry (100 ms exposure, for detection of the P_{RE} transcriptional reporter signal) channels at time intervals of 10 min until cell fate was visible (~2 hr). With time, as infections led to one of the possible pathways, lytic cells were identified by the appearance of YFP fluorescent particles inside the cells, followed by cell lysis. Lysogenic cells were identified by the increased mCherry fluorescence indicating P_{RE} activity. A typical time-lapse movie is shown in Movie S1, and a few snapshots are shown in Figure 1C.

The numbers and positions of phages infecting each cell, as well as cell lengths, were measured manually using MetaMorph. All subsequent data analysis was performed in Matlab (The MathWorks). We performed a total of 24 experiments in which we measured the fates of 2088 cells infected by 4613 phages.

SUPPLEMENTAL INFORMATION

Supplemental Information includes Extended Experimental Procedures, three figures, one table, and one movie and can be found with this article online at doi:10.1016/j.cell.2010.03.034.

ACKNOWLEDGMENTS

We are grateful to A. Campbell, D. Court, J. Cronan, I. Dodd, R. Edgar, M. Elowitz, D. Endy, R. Hendrix, J. Little, R. Moldovan, A. Rokney, F. St-Pierre, P. Thomen, and R.Y. Tsien for generous advice and for providing reagents. We thank members of the Golding, Feiss, and Selvin laboratories for providing help with experiments. We thank A. Arkin, R. Phillips, L. Weinberger, J. Weitz, R. Joh, D. Endy, and F. St-Pierre for commenting on earlier versions of the manuscript. Work in the Golding lab was supported by grants from the National Institutes of Health (R01GM082837-01A1) and Human Frontier Science Program (RGY 70/2008). J.S. and M.F. were supported in part by National Institutes of Health grant GM-51611 and National Science Foundation grant MCB-0717620.

Received: November 19, 2009
Revised: January 25, 2010
Accepted: February 22, 2010
Published: May 13, 2010

REFERENCES

Alberts, B. (2009). Essential Cell Biology, Third Edition (New York: Garland Science).

Alon, U. (2007). An Introduction to Systems Biology: Design Principles of Biological Circuits (Boca Raton, FL: Chapman & Hall/CRC).

Alvarez, L.J., Thomen, P., Makushok, T., and Chatenay, D. (2007). Propagation of fluorescent viruses in growing plaques. Biotechnol. Bioeng. *96*, 615–621.

Arkin, A., Ross, J., and McAdams, H.H. (1998). Stochastic kinetic analysis of developmental pathway bifurcation in phage lambda-infected *Escherichia coli* cells. Genetics *149*, 1633–1648.

Blake, W.J., Kærn, M., Cantor, C.R., and Collins, J.J. (2003). Noise in eukaryotic gene expression. Nature *422*, 633–637.

Blake, W.J., Balazsi, G., Kohanski, M.A., Isaacs, F.J., Murphy, K.F., Kuang, Y., Cantor, C.R., Walt, D.R., and Collins, J.J. (2006). Phenotypic consequences of promoter-mediated transcriptional noise. Mol. Cell *24*, 853–865.

Cagatay, T., Turcotte, M., Elowitz, M.B., Garcia-Ojalvo, J., and Suel, G.M. (2009). Architecture-dependent noise discriminates functionally analogous differentiation circuits. Cell *139*, 512–522.

Cai, L., Friedman, N., and Xie, X.S. (2006). Stochastic protein expression in individual cells at the single molecule level. Nature *440*, 358–362.

Chang, H.H., Hemberg, M., Barahona, M., Ingber, D.E., and Huang, S. (2008). Transcriptome-wide noise controls lineage choice in mammalian progenitor cells. Nature *453*, 544–547.

Choi, P.J., Cai, L., Frieda, K., and Xie, X.S. (2008). A stochastic single-molecule event triggers phenotype switching of a bacterial cell. Science *322*, 442–446.

Chubb, J.R., Trcek, T., Shenoy, S.M., and Singer, R.H. (2006). Transcriptional pulsing of a developmental gene. Curr. Biol. *16*, 1018–1025.

Cohen, J. (2007). Genomics. DNA duplications and deletions help determine health. Science *317*, 1315–1317.

Court, D.L., Oppenheim, A.B., and Adhya, S.L. (2007). A new look at bacteriophage lambda genetic networks. J. Bacteriol. *189*, 298–304.

Edgar, R., Rokney, A., Feeney, M., Semsey, S., Kessel, M., Goldberg, M.B., Adhya, S., and Oppenheim, A.B. (2008). Bacteriophage infection is targeted to cellular poles. Mol. Microbiol. *68*, 1107–1116.

Elowitz, M.B., and Leibler, S. (2000). A synthetic oscillatory network of transcriptional regulators. Nature *403*, 335–338.

Elowitz, M.B., Surette, M.G., Wolf, P.E., Stock, J.B., and Leibler, S. (1999). Protein mobility in the cytoplasm of *Escherichia coli*. J. Bacteriol. *181*, 197–203.

Goldenfeld, N. (1992). Lectures on Phase Transitions and the Renormalization Group (Reading, MA: Addison-Wesley, Advanced Book Program).

Golding, I., Paulsson, J., Zawilski, S.M., and Cox, E.C. (2005). Real-time kinetics of gene activity in individual bacteria. Cell *123*, 1025–1036.

Hecht, M.H., Nelson, H.C., and Sauer, R.T. (1983). Mutations in lambda repressor's amino-terminal domain: implications for protein stability and DNA binding. Proc. Natl. Acad. Sci. USA *80*, 2676–2680.

Hendrix, R.W. (1983). Lambda II (Cold Spring Harbor, NY: Cold Spring Harbor Laboratory Press).

Hershey, A.D. (1971). The Bacteriophage Lambda (Cold Spring Harbor, NY: Cold Spring Harbor Laboratory Press).

Huang, B., Bates, M., and Zhuang, X. (2009). Super-resolution fluorescence microscopy. Annu. Rev. Biochem. *78*, 993–1016.

Kærn, M., Elston, T.C., Blake, W.J., and Collins, J.J. (2005). Stochasticity in gene expression: from theories to phenotypes. Nat. Rev. Genet. *6*, 451–464.

Kobiler, O., Rokney, A., Friedman, N., Court, D.L., Stavans, J., and Oppenheim, A.B. (2005). Quantitative kinetic analysis of the bacteriophage lambda genetic network. Proc. Natl. Acad. Sci. USA *102*, 4470–4475.

Koster, S., Evilevitch, A., Jeembaeva, M., and Weitz, D.A. (2009). Influence of internal capsid pressure on viral infection by phage lambda. Biophys. J. *97*, 1525–1529.

Kourilsky, P. (1973). Lysogenization by bacteriophage lambda. I. Multiple infection and the lysogenic response. Mol. Gen. Genet. *122*, 183–195.

Kourilsky, P., and Knapp, A. (1974). Lysogenization by bacteriophage lambda. III. Multiplicity dependent phenomena occuring upon infection by lambda. Biochimie *56*, 1517–1523.

Lippincott-Schwartz, J., and Patterson, G.H. (2009). Photoactivatable fluorescent proteins for diffraction-limited and super-resolution imaging. Trends Cell Biol. *19*, 555–565.

Locke, J.C., and Elowitz, M.B. (2009). Using movies to analyse gene circuit dynamics in single cells. Nat. Rev. Microbiol. *7*, 383–392.

Longo, D., and Hasty, J. (2006). Dynamics of single-cell gene expression. Mol. Syst. Biol. *2*, 64.

Losick, R., and Desplan, C. (2008). Stochasticity and cell fate. Science *320*, 65–68.

Maamar, H., Raj, A., and Dubnau, D. (2007). Noise in gene expression determines cell fate in *Bacillus subtilis*. Science *317*, 526–529.

Mackay, D.J., and Bode, V.C. (1976). Events in lambda injection between phage adsorption and DNA entry. Virology *72*, 154–166.

Michalowski, C.B., Short, M.D., and Little, J.W. (2004). Sequence tolerance of the phage lambda PRM promoter: implications for evolution of gene regulatory circuitry. J. Bacteriol. *186*, 7988–7999.

Moldovan, R., Chapman-McQuiston, E., and Wu, X.L. (2007). On kinetics of phage adsorption. Biophys. J. *93*, 303–315.

Munoz-Espin, D., Daniel, R., Kawai, Y., Carballido-Lopez, R., Castilla-Llorente, V., Errington, J., Meijer, W.J., and Salas, M. (2009). The actin-like MreB cytoskeleton organizes viral DNA replication in bacteria. Proc. Natl. Acad. Sci. USA *106*, 13347–13352.

Muzzey, D., and van Oudenaarden, A. (2009). Quantitative time-lapse fluorescence microscopy in single cells. Annu. Rev. Cell Dev. Biol. *25*, 301–327.

Neidhardt, F.C., Ingraham, J.L., and Schaechter, M. (1990). Physiology of the Bacterial Cell: A Molecular Approach (Sunderland, MA: Sinauer Associates).

Oppenheim, A.B., Kobiler, O., Stavans, J., Court, D.L., and Adhya, S. (2005). Switches in bacteriophage lambda development. Annu. Rev. Genet. *39*, 409–429.

Ptashne, M. (2004). A Genetic Switch: Phage Lambda Revisited, Third Edition (Cold Spring Harbor, NY: Cold Spring Harbor Laboratory Press).

Raj, A., and van Oudenaarden, A. (2008). Nature, nurture, or chance: stochastic gene expression and its consequences. Cell *135*, 216–226.

Raj, A., Peskin, C.S., Tranchina, D., Vargas, D.Y., and Tyagi, S. (2006). Stochastic mRNA synthesis in mammalian cells. PLoS Biol. *4*, e309.

Russell, J.H., and Keiler, K.C. (2009). Subcellular localization of a bacterial regulatory RNA. Proc. Natl. Acad. Sci. USA *106*, 16405–16409.

Sambrook, J., and Russell, D.W. (2001). Molecular Cloning: A Laboratory Manual, Third Edition (Cold Spring Harbor, NY: Cold Spring Harbor Laboratory Press).

Sherratt, D.J. (2003). Bacterial chromosome dynamics. Science *301*, 780–785.

Singh, A., and Weinberger, L.S. (2009). Stochastic gene expression as a molecular switch for viral latency. Curr. Opin. Microbiol. *12*, 460–466.

Snijder, B., Sacher, R., Ramo, P., Damm, E.M., Liberali, P., and Pelkmans, L. (2009). Population context determines cell-to-cell variability in endocytosis and virus infection. Nature *461*, 520–523.

Spencer, S.L., Gaudet, S., Albeck, J.G., Burke, J.M., and Sorger, P.K. (2009). Non-genetic origins of cell-to-cell variability in TRAIL-induced apoptosis. Nature *459*, 428–432.

St-Pierre, F., and Endy, D. (2008). Determination of cell fate selection during phage lambda infection. Proc. Natl. Acad. Sci. USA *105*, 20705–20710.

Suel, G.M., Kulkarni, R.P., Dworkin, J., Garcia-Ojalvo, J., and Elowitz, M.B. (2007). Tunability and noise dependence in differentiation dynamics. Science *315*, 1716–1719.

Sunshine, M., Feiss, M., Stuart, J., and Yochem, J. (1977). A new host gene (groPC) necessary for lambda DNA replication. Mol. Gen. Genet. *151*, 27–34.

Thanbichler, M., and Shapiro, L. (2008). Getting organized—how bacterial cells move proteins and DNA. Nat. Rev. Microbiol. *6*, 28–40.

Weitz, J.S., Mileyko, Y., Joh, R.I., and Voit, E.O. (2008). Collective decision making in bacterial viruses. Biophys. J. *95*, 2673–2680.

Yamanaka, S. (2009). Elite and stochastic models for induced pluripotent stem cell generation. Nature *460*, 49–52.

Yochem, J., Uchida, H., Sunshine, M., Saito, H., Georgopoulos, C.P., and Feiss, M. (1978). Genetic analysis of two genes, dnaJ and dnaK, necessary for *Escherichia coli* and bacteriophage lambda DNA replication. Mol. Gen. Genet. *164*, 9–14.

Yu, J., Xiao, J., Ren, X., Lao, K., and Xie, X.S. (2006). Probing gene expression in live cells, one protein molecule at a time. Science *311*, 1600–1603.

Zanghi, C.N., Lankes, H.A., Bradel-Tretheway, B., Wegman, J., and Dewhurst, S. (2005). A simple method for displaying recalcitrant proteins on the surface of bacteriophage lambda. Nucleic Acids Res. *33*, e160.